# In Situ Epitaxial Growth of Triangular CdS Nanoplates on Mica by Dip-Pen Nanolithography

**Haibin Chu,[†] Lei Ding,[†] Jinyong Wang,[†] Xuemei Li,[†] Liping You,[‡] and Yan Li*,[†]**

*Beijing National Laboratory for Molecular Sciences, Key Laboratory for the Physics and Chemistry of Nanodevices, National Laboratory of Rare Earth Material Chemistry and Application, College of Chemistry and Molecular Engineering, and Electron Microscopy Laboratory, Peking University, Beijing 100871, China*

*Received: August 31, 2008; Revised Manuscript Received: September 23, 2008*

Epitaxial growth of triangular CdS nanoplates by dip-pen nanolithography is achieved on a mica substrate. This method offers in situ initiating, controlling, and monitoring of the epitaxial growth of triangular CdS plates in nanoscale. Control experiments and structure analysis indicate that both the tip-modulated crystallization and matching in the crystal structures (symmetry and lattice) of CdS and mica play key roles in the epitaxial growth of well-crystallized CdS nanostructures.



## 1. Introduction

The fabrication of nanostructures composed of functional inorganic materials is very important for building various nanodevices.[1−3] Both the high-resolution and in situ monitoring for nanomanipulation[4] and fabrication of nanodevices[5−11] have enabled the scanning probe lithography (SPL) based technique,[12−14] a powerful tool for patterning inorganic nanostructures on surfaces. Dip-pen nanolithography (DPN),[15,16] which is an active member in the SPL family, can directly generate nanostructures of inorganic materials by transferring inorganic species from AFM tips onto various substrates. Nanostructures made of inorganic materials, such as metals,[17−21] oxides,[22,23] chalcogenides,[24,25] and even complicated magnetic compounds,[7,26] have been fabricated on substrates by DPN. Moreover, DPN-generated patterns of organic molecules can be used as templates for directed assembly of various inorganic nanomaterials, such as carbon nanotubes[27,28] and nanowires,[29] and served as etching resists for the fabrication of inorganic nanostructures.[30−34] The DPN method possesses the advantages of very high resolution, registration, and flexibility.[16,35] However, the inorganic materials generated directly by DPN were normally in poor crystallization. Using DPN or other SPL methods to directly fabricate single-crystalline inorganic materials, which often show better performance than amorphous or polycrystalline materials in various applications,[36] is still a big challenge.

Moreover, DPN is the only potential tool available for simultaneously initiating and visualizing the very beginning step of the crystallization process at nanometer scale,[37] thus facilitating the in situ study of the nucleation and growth process in the crystallization of various materials. Other characterization instruments such as spectroscopic or X-ray diffraction tools could only observe the crystallization process of crystals with a size larger than 100 $\mu m^3$.[38] However, there is only one report showing that DPN can be used to in situ induce and record the nucleation and crystal growth of poly-DL-lysine hydrobromide (PLH) single crystals on mica.[37] Until now, there is still no report about the site-controlled initiating and monitoring for the crystal growth of inorganic materials by DPN.

Epitaxial growth of single crystalline inorganic materials on the surface has been explored as a useful technique for substrate engineering and fabricating a wide range of nanostructures and devices.[39,40] CdS is an important inorganic semiconductor.[41] Mica has been used as the substrate for epitaxial growth of CdS films in solution.[42] We demonstrated previously that CdS nanostructures could be patterned on mica by DPN using cadmium acetate and thioacetamide (TAA) as ink.[24] Here, we further report that, by carefully controlling the DPN conditions, nucleation and epitaxial growth of equilateral triangular CdS nanoplates on mica can be achieved by DPN. The regular structure of the triangles indicated that they were well crystallized. Investigation on the crystal structures of mica and CdS revealed that epitaxial growth of the triangular CdS nanoplates on mica was due to the matching both in symmetry and lattice. As far as we know, it is the first time to initiate inorganic crystal nucleation and to control and to monitor the growth process on substrates by DPN.

## 2. Experimental

All chemicals used are of analytical grade. In a typical process, the silicon AFM probe (CSG11 purchased from NT-MDT Co. with a nominal spring constant of 0.01−0.08 N $m^{-1}$) was inked for 10 s with freshly mixed ethanol solution of 1 mM $Cd(Ac)_2$ and 1 mM TAA as previously reported[24] and blown dry with high-purity nitrogen. Then, the probe was mounted on a SPA400 SPM (Seiko Instrument Inc.) and operated in contact mode for deposition of CdS onto a freshly cleaved mica substrate. A small contact force of 0.05 nN was used for DPN deposition to avoid damage to the sample. The inked tip was used to scan across the mica substrate over an area of 4 × 4 $\mu m^2$ at the scan rate of 2 Hz for several times at a relative humidity of 25−35% and room temperature unless pointed out otherwise. After the DPN process, another AFM probe (NSG11 purchased from NT-MDT Co.) was used for imaging in the tapping mode at a relative humidity of 10−20% one day after the DPN process. The relative humidity, measured with a digital hygrometer, was adjusted by a humidifier and a

* Author to whom correspondence should be addressed. Phone/fax: +86-10-62756773. E-mail: yanli@pku.edu.cn.
[†] Beijing National Laboratory for Molecular Sciences, Key Laboratory for the Physics and Chemistry of Nanodevices, National Laboratory of Rare Earth Material Chemistry and Application, College of Chemistry and Molecular Engineering.
[‡] Electron Microscopy Laboratory.

10.1021/jp807746g CCC: $40.75 
Published on Web 11/11/2008

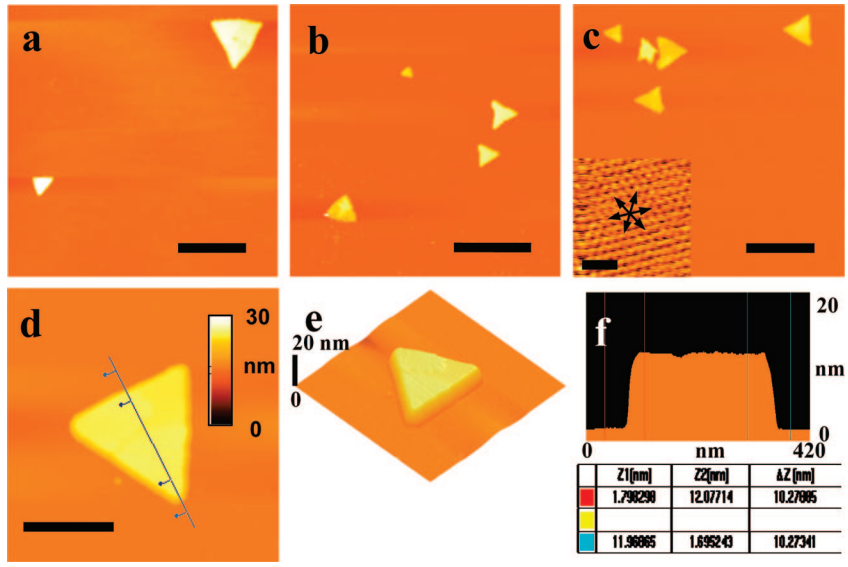


**Figure 1.** Topographical images (a−d) of triangular CdS nanoplates formed by DPN on mica. The corresponding 3D image (e) and height profile (f) of Figure (d) show the flatness of the triangle. The triangle was fabricated by continuously scanning an AFM tip coated by $Cd(Ac)_2$ and TAA in contact mode with a scan size of $4 \times 4\ \mu m^2$ and scan rate of 2 Hz several times. The images were collected with a clean AFM tip in tapping mode. The color bar in (d) fits for images (a−d). The scale bars in (a−c) = 1 $\mu$m, and the scale bar in (d) = 200 nm. The inset image of (c) is the mica atomic image before AFM writing, and the scale bar in the inset of (c) = 3 nm.



dehumidifier. Copper grids were put on mica substrates to be used as micron-scaled registration markers for collecting scanning transmission electron microscopic (STEM) images and corresponding EDX spectra (Philips Tecnai F30 FEG-TEM operating at 300 kV) from a specific region. The prepared CdS triangles in an area of $100 \times 100\ \mu m^2$ were characterized with XPS (Kratos Axis Ultra).

## 3. Results and Discussions

Figure 1 shows the typical atomic force microscopy (AFM) images of the triangular CdS nanoplates fabricated by DPN. Most nanoplates were flat equilateral triangles with an edge length of 100−2000 nm and height of 5−25 nm. The 3D image in Figure 1e and the corresponding height profile in Figure 1f of a triangular nanoplate both indicate its smooth surface. The regular edges and uniform heights of the nanoplates suggested that the triangles were well crystallized and should be single crystals. The atomic resolution image in the inset of Figure 1c shows the hexagonal symmetry of the underlying mica substrate. The symmetry consistency of mica with wurtzite CdS might play an important role in the formation of triangular CdS nanoplates. Moreover, most of the triangular nanoplates lay in two opposite directions that differed by 180° to each other, and these directions had no relation with the scan direction. These pieces of evidence all indicate the epitaxial growth of CdS nanoplates on mica.

The triangular nanoplates became very stable for tapping-mode AFM imaging after several hours of aging and could maintain over a week. This is quite different from the PLH single crystals formed on mica which lost water and changed morphology when dried in air.[37] In addition, the triangular nanoplates were stable against rinsing by water. This demonstrated that they were not $Cd(Ac)_2$ or TAA. Energy dispersive X-ray (EDX) spectroscopy and X-ray photoelectron spectroscopy (XPS) were used to investigate the composition of the triangles. Figures 2b and 2c show two EDX spectra taken from the corresponding areas in Figure 2a, respectively. They together show clearly that sulfur only existed in the area with deposited triangles. The existence of cadmium in the triangles was difficult to identify because of the high counts of potassium from the mica substrate. XPS is a useful technique to obtain information about the surface chemical compositions of the samples.[24] Figures 2d and 2e are the XPS spectra of the 2p region of sulfur taken in the areas with and without triangles, respectively. The results from the deconvolution analysis were also shown in Figure 2d. The two fitting curves correspond to the 2p3/2 (peak at 162.40 eV) and the 2p1/2 (peak at 163.58 eV) of sulfur, respectively. The Cd 3d peak was not observed because the very weak signal from such small amount of CdS was well covered by the high background signal. However, the binding energy peak of S 2p3/2 is in good accordance with the reported data of 162.2 eV for S 2p3/2 of CdS.[43] Therefore, the EDX and XPS data reveal that the nanoplates obtained on mica are made of CdS.

Figure 3 shows a series of AFM images along with the DPN process by bringing an AFM tip coated with $Cd(Ac)_2$ and TAA into contact with the mica substrate in an area of $4 \times 4\ \mu m^2$ with a scan rate of 2 Hz. While the tip was scanned across the same area, the growth of the triangles was observed in both edge length and height. A newly formed nucleus was also found after the fifth scan (as indicated by 'D' in Figure 3a). The evolution of the edge length (Figure 3b), height (Figure 3c), top surface area (Figure 3d), and volume (Figure 3e) of the triangles A, B, C, and D gave quantitative crystal growth information during the continuous AFM writing. Figure 3b and Figure 3c show that the growth rate of the edge length (4−22 nm per scan) was much faster than that of the height of the triangles (0.05−1.56 nm per scan). This may be mainly due to the strong electrostatic interaction between the positively charged CdS species and the negatively charged mica surface.[24] In addition, the edge length of the triangles increased much faster in the first few scans than the last few ones. For example, the average growth rate of the edge length of triangle A was 22 nm per scan during the first seven scans and decreased to 4 nm per scan during the last five scans. For the newly nucleated triangle D, the average growth rate of the edge length was 19 nm per scan during the first six writings (scan times from 5 to 11 in Figure 3b), and the growth rate dropped to 4 nm per scan

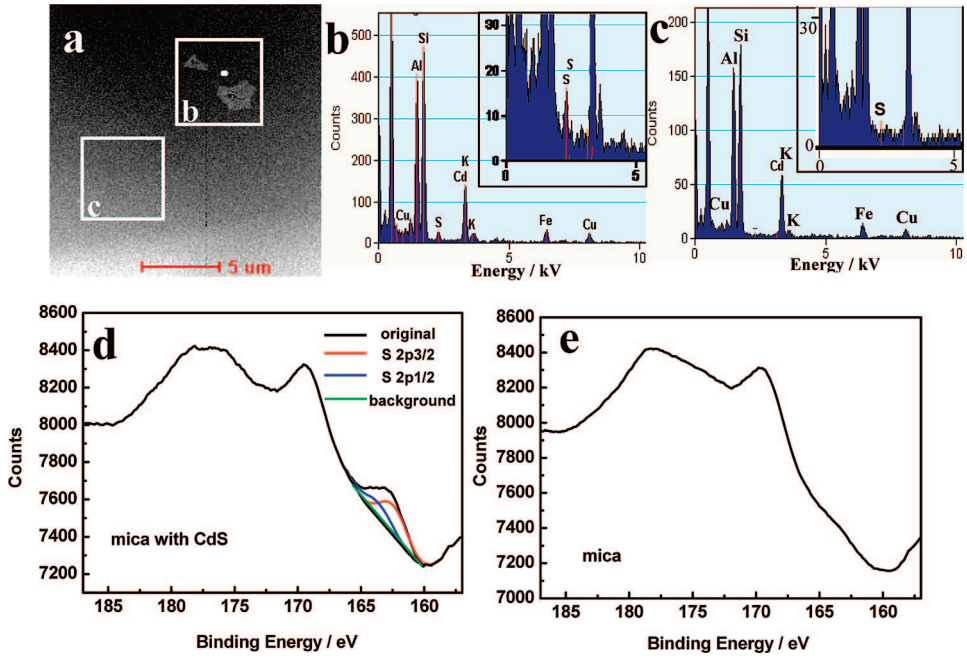


**Figure 2.** (a) STEM image of the produced CdS on mica. (b) and (c) are EDX spectra corresponding to the two solid rectangular frames in (a), respectively. Insets in (b) and (c) are the magnifications of the corresponding spectra. (d) and (e) are the XPS spectra of the S 2p region of the area with and without CdS triangles, respectively. The black curves in (d) and (e) are the original signals. The red and blue curves in (d) are the results of the XPS surface deconvolution analysis for S 2p, which are corresponding to S 2p3/2 and S 2p1/2, respectively. The green line is the background signal.



during the last four writings. Besides, the heights of triangles A, B, and C increased at a rate of 0.07−0.10 nm per scan; i.e., the CdS triangles increased one unit cell (~0.6 nm) in height every 6 to 9 scans. The growth rate is comparable to the epitaxial growth rate of CdS films on mica in solution, which is one unit cell in 3 min.[42] However, the height of the newly nucleated triangle D increased at a much faster rate of 1.56 nm (about three unit cells) per scan during the first three scans, and the growth rate decreased to 0.05 nm (i.e., 1/12 of one unit cell) per scan soon (scan times from 7 to 20 in Figure 3b). The volume of the triangles increased almost at a constant rate in the first 20 scans (Figure 3e). This indicated that the amount of CdS species transferred from the AFM tip to substrate was almost equal during each scan. However, the growth rate of the top surface area and volume of the triangles slowed down during the last three scans (Figure 3e). Besides, we should point out that the nucleation process was relatively slow. Triangular CdS nanoplates came up sometimes in the first scan, but for most cases, two to ten scans were needed before the appearance of nanoplates. Moreover, some newly nucleated nanoplates, for instance, triangle D in Figure 3a, may occur during the growth process of other plates. It was concluded from the above information that the crystal growth kinetics of triangular CdS nanoplates on mica could be divided into three stages: slow nucleation process, followed by fast growth process, and finally slow ripeness process. This is similar to the crystal growth behavior in bulk solution.[44]

We have shown that DPN can be used to initiate, monitor, and examine the crystallization of CdS on mica. Further experiments illuminated that this method can also control the location where the nanoplates were formed by controlling the movement of the AFM tip. The site-specific accuracy in one dimension is at the submicro scale (Figure S1 in Supporting Information).

We systematically studied the effect of scan mode, relative humidity, and properties of substrates on the growth of CdS. The AFM was operated in contact mode during the DPN process. The comparative experiments operated in tapping mode did not result in the formation of CdS features. As it may take some time for the reaction to form CdS, the contacting time in tapping mode might be too short for the formation of CdS on mica. However, under contact mode, the AFM tip must be operated with a small contact force of ~0.05 nN to avoid damage to the CdS crystals formed on mica. In addition, the relative humidity was very important for fabricating triangular CdS nanoplates. In our previous report,[24] continuous CdS nanowires were created at a relative humidity of 40−55% with a translate rate below 120 nm/s, whereas for epitaxial growth of triangular CdS nanoplates, when the inked AFM tip was scanned across the mica substrate over a $4 \times 4\ \mu m^2$ area at the scan rate of 2 Hz (i.e., 16 $\mu$m/s), the optimal relative humidity was 25−35% at room temperature. When the relative humidity was lower than 20%, CdS nanocrystals were hardly obtained on mica, but if the relative humidity was higher than 40%, only nearly spherical nanocrystals were formed (Figure S2 in Supporting Information). The relative humidity at 25−35% may provide the proper amount and supersaturation of precursors in the tip meniscus for the crystallization and formation of triangular CdS nanoplates.

It is known that the properties of the substrates play important roles in all epitaxial growth processes.[45] In our DPN-based process, it was found that the freshly cleaved mica was very suitable for epitaxial growth of triangular CdS nanoplates. If mica was exposed in air for a long time or immersed in water before DPN writing, CdS nanoplates were seldom obtained on it. We also performed the similar DPN process on other substrates including H-terminated silicon wafers and silicon wafers with a native or thermal oxide layer (Figure S3 in Supporting Information). No particles formed on H-terminated silicon wafers, and only nanoparticle arrays were deposited on silicon wafers with the native or thermal oxide layer because of the electrostatic interaction resulting from the charge separation caused by the friction between the AFM tip and the substrate.[23]

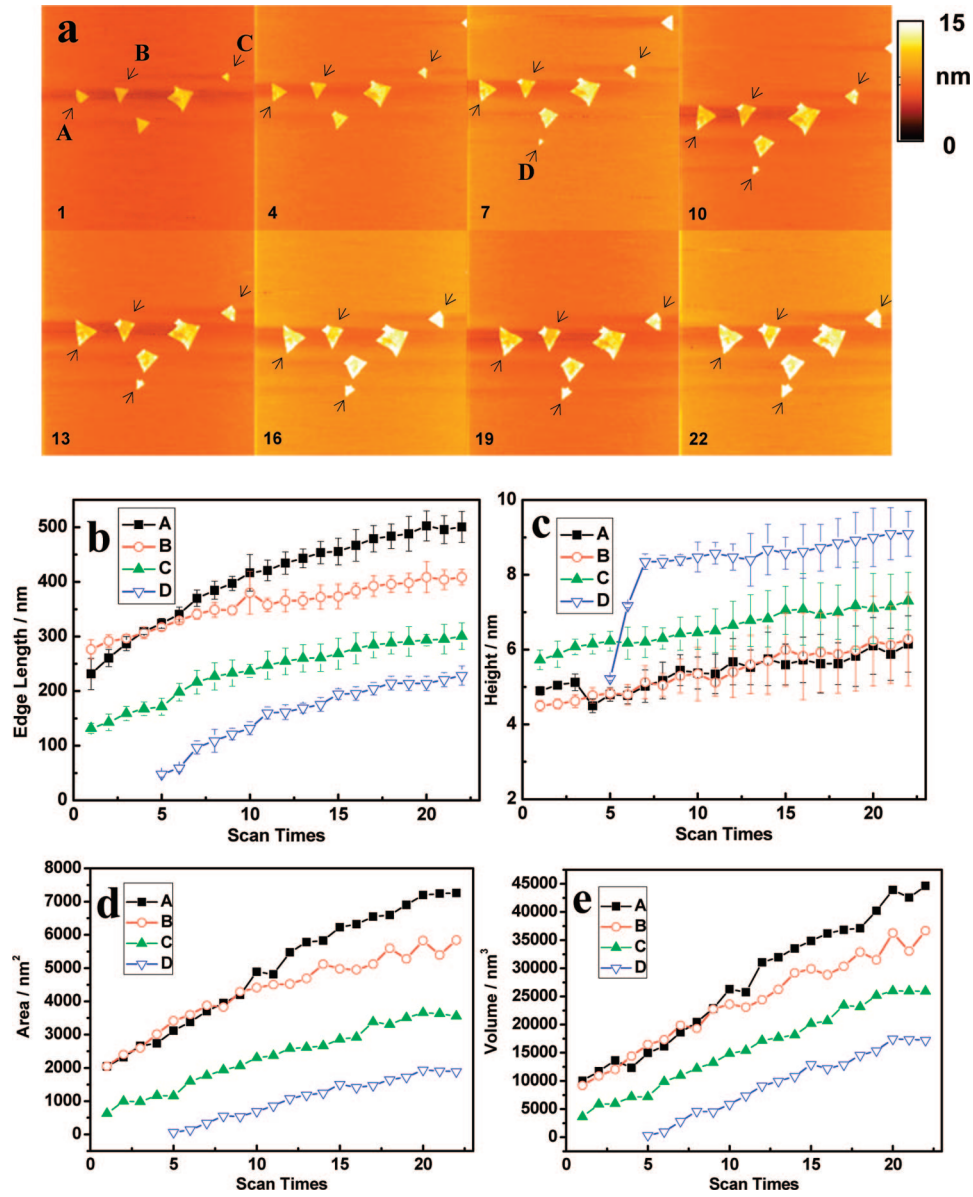


**Figure 3.** (a) Topographical images showing a series of 4 × 4 $\mu m^2$ panels obtained by in situ writing with an AFM tip coated with $Cd(Ac)_2$ and TAA in contact mode with a scan rate of 2 Hz after 1, 4, 7, 10, 13, 16, 19, and 22 times writing, respectively. The fields of panels 4, 7, and 10 are slightly offset due to thermal shift. (b−e) are edge length, height, top surface area, and volume evolution, respectively, of the features indicated by characters in (a) during the 22 times of writing.

It has been reported that flat triangular CdS nanocrystals can be synthesized through colloidal pathways.[46−48] We immersed freshly cleaved mica substrates in the mixed solution of $Cd(Ac)_2$ and TAA for 3−60 min at temperatures varying from 18 to 60 °C. The solvents of the solutions were water, ethanol, or a mixture of the two, and the concentrations of $Cd(Ac)_2$ and TAA varied from 1 to 4 mM. Films composed of irregular CdS islands instead of flat triangles were formed on mica substrates for all the comparative experiments in solution. This indicates that the tip-modulated process obtained the crucial crystallization condition for the growth of triangular CdS nanoplates on mica. The suitable supersaturation of CdS species in the meniscus between the AFM tip and the mica substrate provided an opportunity for heteroepitaxial growth, and the presence of a mica surface helped to increase the nucleation rate of CdS epitaxial growth.[39]

Further investigation on the surface structure shed light on the possible mechanism for the epitaxial growth of triangular CdS nanoplates on mica. First, the (001) plane of mica shows the pseudohexagonal structure (Figure 4a), which symmetrically matches the (0001) plane of wurtzite CdS (Figure 4b). Second, the lattice misfit of $4d_{200}$(mica) and $5d_{110}$(CdS) is 0.3% (corresponding to the horizontal dotted line in Figure 4c), and the lattice misfit of $4d_{220}$(mica) and $5d_{200}$(CdS) is 0.1% (corresponding to the tilted dotted line in Figure 4c). The lattice misfit is quite small. Therefore, the difference of chemical potentials of the deposited crystals and substrate in epitaxial growth is due mainly to the difference in bond strengths of CdS and mica.[44] CdS triangular crystals may stand on mica via Cd−O bonds. On the basis of the above comparative experiments and structure analysis, the possible mechanism for the generation of triangular CdS nanoplates by DPN was proposed. The tip-modulated crystallization process provided supersaturation of CdS in the meniscus that favored heteroepitaxial growth,[39] and the electrostatic force between the CdS building units and the substrate was the main driving force for the growth of CdS on mica. Moreover, the matching in both symmetry and lattice led to the epitaxial growth of triangular CdS nanoplates. The epitaxial orientation was $(0001)\langle 0001\rangle_{CdS} \| (001)\langle 001\rangle_{mica}$;

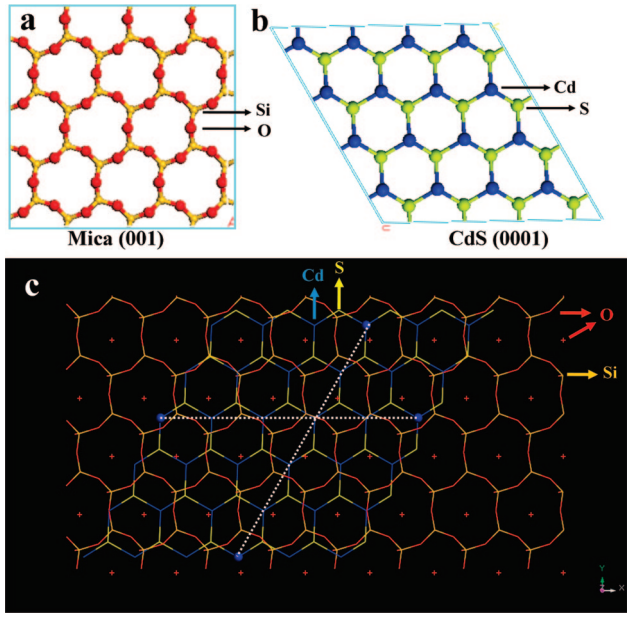


**Figure 4.** Scheme of the surface crystal structures. (a) (001) plane of mica (muscovite). (b) (0001) plane of wurtzite CdS. (c) (0001) plane of wurtzite CdS on (001) plane of mica.

i.e., the CdS plane in contact with mica (001) was (0001), and the CdS <0001> direction was parallel to the direction <001> of mica. Hence, triangular CdS nanoplates should grow along two opposite directions, which resulted in the triangles parallel or antiparallel to each other.

## 4. Conclusion

In conclusion, we developed a DPN method to in situ initiate and control the epitaxial growth of triangular CdS nanoplates on the mica surface. Comparative experiments and structure analysis indicated that both the tip-modulated crystallization and the matching in the crystal structures (symmetry and lattice) of the CdS and mica substrate played key roles in epitaxial growth of the well-crystallized triangular CdS nanoplates. This DPN-based method could be extended to directly fabricate well-crystallized CdS or other inorganic nanostructures on various functional single crystals, such as GaN, InP, and GaAs, which are of great interest for future optoelectronic applications.[45] This strategy would also open up possibilities for studying the very beginning stage of the epitaxial growth of inorganic crystals on substrates.

**Acknowledgment.** This work was supported by NSF (Project 90406018) and MOST (Projects 2007CB936202, 2006CB932403, and 2006CB932701) of China.

**Supporting Information Available:** AFM images of CdS nanoplates generated by site-specific placement, as well as CdS nanostructures formed at high relative humidity and on different substrates. This material is available free of charge via the Internet at http://pubs.acs.org.

## References and Notes

(1) Xia, Y. N.; Yang, P. D.; Sun, Y. G.; Wu, Y. Y.; Mayers, B.; Gates, B.; Yin, Y. D.; Kim, F.; Yan, Y. Q. *Adv. Mater.* **2003**, *15*, 353.
(2) Gates, B. D.; Xu, Q. B.; Stewart, M.; Ryan, D.; Willson, C. G.; Whitesides, G. M. *Chem. Rev.* **2005**, *105*, 1171.
(3) Woodson, M.; Liu, J. *Phys. Chem. Chem. Phys.* **2007**, *9*, 207.
(4) Sugimoto, Y.; Abe, M.; Hirayama, S.; Oyabu, N.; Custance, O.; Morita, S. *Nat. Mater.* **2005**, *4*, 156.
(5) Campbell, P. M.; Snow, E. S.; McMarr, P. J. *Appl. Phys. Lett.* **1995**, *66*, 1388.
(6) Schumacher, H. W.; Keyser, U. F.; Zeitler, U.; Haug, R. J.; Eberl, K. *Appl. Phys. Lett.* **1999**, *75*, 1107.
(7) Fu, L.; Liu, X. G.; Zhang, Y.; Dravid, V. P.; Mirkin, C. A. *Nano Lett.* **2003**, *3*, 757.
(8) Fuhrer, A.; Luescher, S.; Ihn, T.; Heinzel, T.; Ensslin, K.; Wegscheider, W.; Bichler, M. *Nature* **2001**, *413*, 822.
(9) Rosa, J. C.; Wendel, M.; Lorenz, H.; Kotthaus, J. P.; Thomas, M.; Kroemer, H. *Appl. Phys. Lett.* **1998**, *73*, 2684.
(10) Irmer, B.; Blick, R. H.; Simmel, F.; Godel, W.; Lorenz, H.; Kotthaus, J. P. *Appl. Phys. Lett.* **1998**, *73*, 2051.
(11) Su, M.; Li, S. Y.; Dravid, V. P. *J. Am. Chem. Soc.* **2003**, *125*, 9930.
(12) Nyffenegger, R. M.; Penner, R. M. *Chem. Rev.* **1997**, *97*, 1195.
(13) Liu, G. Y.; Xu, S.; Qian, Y. L. *Acc. Chem. Res.* **2000**, *33*, 457.
(14) Kramer, S.; Fuierer, R. R.; Gorman, C. B. *Chem. Rev.* **2003**, *103*, 4367.
(15) Piner, R. D.; Zhu, J.; Xu, F.; Hong, S. H.; Mirkin, C. A. *Science* **1999**, *283*, 661.
(16) Ginger, D. S.; Zhang, H.; Mirkin, C. A. *Angew. Chem., Int. Ed.* **2004**, *43*, 30.
(17) Li, Y.; Maynor, B. W.; Liu, J. *J. Am. Chem. Soc.* **2001**, *123*, 2105.
(18) Maynor, B. W.; Li, Y.; Liu, J. *Langmuir* **2001**, *17*, 2575.
(19) Ben Ali, M.; Ondarcuhu, T.; Brust, M.; Joachim, C. *Langmuir* **2002**, *18*, 872.
(20) Thomas, P. J.; Kulkarni, G. U.; Rao, C. N. R. *J. Mater. Chem.* **2004**, *14*, 625.
(21) Prime, D.; Paul, S.; Pearson, C.; Green, M.; Petty, M. C. *Mater. Sci. Eng., C* **2005**, *25*, 33.
(22) Su, M.; Liu, X. G.; Li, S. Y.; Dravid, V. P.; Mirkin, C. A. *J. Am. Chem. Soc.* **2002**, *124*, 1560.
(23) Ding, L.; Li, Y.; Chu, H. B.; Li, C. Q.; Yang, Z. H.; Zhou, W. W.; Tang, Z. K. *Appl. Phys. Lett.* **2007**, 91.
(24) Ding, L.; Li, Y.; Chu, H. B.; Li, X. M.; Liu, J. *J. Phys. Chem. B* **2005**, *109*, 22337.
(25) Roy, D.; Munz, M.; Colombi, P.; Bhattacharyya, S.; Salvetat, J. P.; Cumpson, P. J.; Saboungi, M. L. *Appl. Surf. Sci.* **2007**, *254*, 1394.
(26) Gundiah, G.; John, N. S.; Thomas, P. J.; Kulkarni, G. U.; Rao, C. N. R.; Heun, S. *Appl. Phys. Lett.* **2004**, *84*, 5341.
(27) Rao, S. G.; Huang, L.; Setyawan, W.; Hong, S. H. *Nature* **2003**, *425*, 36.
(28) Wang, Y. H.; Maspoch, D.; Zou, S. L.; Schatz, G. C.; Smalley, R. E.; Mirkin, C. A *Proc. Natl. Acad. Sci. U.S.A.* **2006**, *103*, 2026.
(29) Myung, S.; Im, J.; Huang, L.; Rao, S. G.; Kim, T.; Lee, D. J.; Hong, S. H. *J. Phys. Chem. B* **2006**, *110*, 10217.
(30) Zhang, H.; Li, Z.; Mirkin, C. A. *Adv. Mater.* **2002**, *14*, 1472.
(31) Weinberger, D. A.; Hong, S. G.; Mirkin, C. A.; Wessels, B. W.; Higgins, T. B. *Adv. Mater.* **2000**, *12*, 1600.
(32) Zhang, H.; Chung, S. W.; Mirkin, C. A. *Nano Lett.* **2003**, *3*, 43.
(33) Salaita, K. S.; Lee, S. W.; Ginger, D. S.; Mirkin, C. A. *Nano Lett.* **2006**, *6*, 2493.
(34) Zhang, H.; Amro, N. A.; Disawal, S.; Elghanian, R.; Shile, R.; Fragala, J. *Small* **2007**, *3*, 81.
(35) Salaita, K.; Wang, Y. H.; Mirkin, C. A. *Nat. Nanotechnol.* **2007**, *2*, 145.
(36) Comini, E. *Anal. Chim. Acta* **2006**, *568*, 28.
(37) Liu, X. G.; Zhang, Y.; Goswami, D. K.; Okasinski, J. S.; Salaita, K.; Sun, P.; Bedzyk, M. J.; Mirkin, C. A. *Science* **2005**, *307*, 1763.
(38) Pluth, J. J.; Smith, J. V.; Pushcharovsky, D. Y.; Semenov, E. I.; Bram, A.; Riekel, C.; Weber, H. P.; Broach, R. W *Proc. Natl. Acad. Sci. U.S.A.* **1997**, *94*, 12263.
(39) Ayers, J. E. *Heteroepitaxy of Semiconductors: Theory, Growth, and Characterization*; CRC Press: Boca Raton, 2007.
(40) Amano, H.; Sawaki, N.; Akasaki, I.; Toyoda, Y. *Appl. Phys. Lett.* **1986**, *48*, 353.
(41) Chu, H. B.; Li, X. M.; Chen, G. D.; Zhou, W. W.; Zhang, Y.; Jin, Z.; Xu, J. J.; Li, Y. *Cryst. Growth Des.* **2005**, *5*, 1801.
(42) Breen, M. L.; Woodward, J. T.; Schwartz, D. K.; Apblett, A. W. *Chem. Mater.* **1998**, *10*, 710.
(43) Houng, M. P.; Fu, S. L.; Wu, T. S. *J. Mater. Sci. Lett.* **1986**, *5*, 96.
(44) Markov, I. V. *Crystal Growth for Beginners: Fundamentals of Nucleation, Crystal Growth and Epitaxy*; World Scientific: Singapore, 1995.
(45) Froment, M.; Bernard, M. C.; Cortes, R.; Mokili, B.; Lincot, D. *J. Electrochem. Soc.* **1995**, *142*, 2642.
(46) Pinna, N.; Weiss, K.; Urban, J.; Pileni, M. P. *Adv. Mater.* **2001**, *13*, 261.
(47) Pinna, N.; Weiss, K.; Sack-Kongehl, H.; Vogel, W.; Urban, J.; Pileni, M. P. *Langmuir* **2001**, *17*, 7982.
(48) Warner, J. H.; Tilley, R. D. *Adv. Mater.* **2005**, *17*, 2997.

JP807746G